



Catalytic Nanomedicine: Coated bionanocatalysts for Catalytic Antineoplastic activity

Tessy López-Goerne¹ · Emma Ortiz-Islas² · Francisco Rodríguez-Reinoso³ · Hugo Monroy² · Esteban Gómez-López⁴ · Francisco J. Padilla-Godínez^{1,5}

Received: 4 April 2024 / Revised: 15 May 2024 / Accepted: 22 May 2024 / Published online: 16 June 2024
© The Author(s) 2024

Abstract

Glioma tumors are the most common form of central nervous system tumors, and there is a pressing need for innovative methods that can precisely target cancer cells while leaving healthy tissues unharmed. In this study, progressing in the field of Catalytic Nanomedicine, we investigated the cytotoxic effects of a novel class of bionanocatalysts on glioma cancer cells. These bionanocatalysts were constructed from a catalytic matrix of oxides with evenly dispersed superficial copper-coating nanoparticles. This design optimizes both the inherent catalytic characteristics of the matrix and instills cytotoxic properties. The bionanocatalysts coated with copper demonstrated a significant reduction in cancer cell viability when compared to reference bionanocatalysts without the transition metal. We also observed structural damage to the cytoskeleton and alterations in mitochondrial activity. These findings suggest that these pathways are integral to the mechanisms through which these nanostructures execute their bionanocatalytic activities, particularly in breaking chemical bonds. Importantly, our physicochemical analyses verified that the coating with copper species, primarily CuO, did not disrupt the individual structure of the bionanocatalysts: instead, it enhanced their catalytic cytotoxic potential. This research aims to deepen our understanding of the mechanisms underlying this promising antineoplastic treatment and underscore the effectiveness of superficial copper-coating nanoparticles as agents for amplifying the inherent properties of bionanocatalysts through nanocatalysis.

Keywords Catalytic nanomedicine · Bionanocatalyst · Glioblastoma multiforme · XPS · Cytotoxic · Histology

1 Introduction

Glial tumors stand out as the most prevalent type of central nervous system tumors [44]. Within this category, glioblastoma multiforme represents the most aggressive and malignant form of glioma, posing a formidable challenge as one of the most aggressive and incurable cancers [48], with an average survival of just 12 to 15 months [39]. The limitations of surgical resection in completely eliminating malignant cells [49], coupled with the extensive side effects associated with chemotherapy [56], have spurred research into innovative approaches for selectively targeting cancer cells. Among these recent strategies, antineoplastic bionanocatalysts have emerged as a highly promising avenue [20]. Their appeal lies in several key attributes: their diminutive nanoscale size (typically < 100 nm), expansive surface area, selectivity, mesoporous structure, and catalytic activity, particularly in selectively cleaving essential molecular bonds, such as those within DNA [19].

✉ Tessy López-Goerne
tessy3@prodigy.net.mx

¹ Laboratory of Nanotechnology and Nanomedicine, Department of Health Care, Metropolitan Autonomous University, Coyoacan, Mexico City 04960, Mexico

² Laboratory of Nanotechnology, National Institute of Neurology and Neurosurgery, Mexico City 14269, Mexico

³ Advanced Materials Laboratory, University of Alicante, Alicante 03690, Spain

⁴ AG Nanooptik, Humboldt-Universität zu Berlin, 10117 Berlin, Germany

⁵ Department of Mathematics and Physics, Western Institute of Technology and Higher Education, San Pedro Tlaquepaque 45604, Mexico

Bionanocatalysts consist of an oxide matrix where nanostructured metallic agents are uniformly dispersed on its surface, orchestrating a harmonious synergy with the matrix [30]. These nanostructures are adept at catalyzing the selective breakdown of carbon-carbon and carbon-nitrogen bonds by lowering the activation energy required for the process [10, 52, 57]. Of significant note, these nanostructures are engineered for precision, exerting their catalytic influence specifically on the bonds found within genetic material, including DNA and RNA [30]. Moreover, the surface of bionanocatalysts is thoughtfully functionalized with organic agents, rendering these structures inherently and selectively biocompatible exclusively for cancer cells while preserving the integrity of surrounding healthy tissues [24, 26].

In this endeavor, we have synthesized a distinct variant of bionanocatalyst, rooted in a composite matrix of titanasilicate (TiSiO_x), where copper-coated nanoparticles have been adroitly dispersed on its surface. Notably, these nanoparticles have demonstrated a remarkable capability to effectively diminish the viability of glioma cells. The physicochemical and structural properties of these innovative bionanocatalysts are meticulously examined through a range of characterization techniques, paving the way for an enhanced understanding of their potential in Catalytic Nanomedicine for cancer treatment.

2 Experimental procedure

2.1 Synthesis of coated bionanocatalysts

Bionanocatalysts were synthesized following a previously reported protocol [26]. Briefly, matrix precursors were added dropwise to solution of deionized water and refluxed at 70 °C until gelation of the matrix: the gel was evaporated until the obtention of a powder. Then, for coating, the appropriate amount of copper precursor ($\text{Cu}(\text{acac})_2$) was dissolved in deionized water and organic functionalizing agents, in which the already synthesized powder matrix was added. The amount of coating copper was established following the results of previous studies in which different concentrations of copper were evaluated (from 10 to 1%) [4]. Solvents were evaporated until fine powder obtention, which was subjected to a manual grinding process in an Agate mortar.

2.2 Bionanocatalysts characterization

X-ray photoelectron spectroscopy (XPS) spectra was obtained using a PHI 5700 spectrometer (Physical Electronics, MN, USA) with a non-monochromatic Mg $K\alpha$ radiation (300 W, 15 kV, $h\nu = 1253.6$ eV) as excitation source (pass

energy mode at 25.9 eV, chamber kept below 10^{-7} Pa). Charge referencing was done against adventitious carbon (C 1s at 284.8 eV). PHI ACCESS ESCA-V6.0 F and Multipack 8.2b software packages were used for acquisition and data analysis. Short acquisition times (< 10 min) were used in order to avoid the photoreduction of the Cu species [45]. N_2 adsorption-desorption isotherms were generated through the utilization of a Micromeritics Belsorp IIBell Japan INC instrument. The surface area was determined via the application of the Brunauer-Emmett-Teller (BET) methodology, while the pore volume and pore size distribution were assessed using the Barrett-Joyner-Halenda (BJH) approach. The size, shape, and texture of the grains were analyzed using a JEOL JSM-6010LV scanning electron microscope (SEM). The size of the particles in the samples was assessed through Transmission Electron Microscopy (TEM). Micrographs were captured using a JEOL JEM-2100 F electron microscope, operating with a 200 kV accelerated electron beam. FTIR spectra acquisition was conducted using a NICOLET FTIR spectrometer, specifically the MAGNA 560 model, which featured a resolution of 4 cm^{-1} . A total of 100 scans were averaged for each measurement.

2.3 Cell culture

The Rat C6 glioma cell line was acquired from the European Collection of Animal Cell Cultures located in Porton Down, UK. These cells were cultured in 60-mm Petri dishes using an F-12 Ham Nutrient Mixture, which was supplemented with 10% FBS Gold serum, 2 mM glutamine, 100 U/ml penicillin, and 100 $\mu\text{g/ml}$ streptomycin. This culture was maintained in a humid environment consisting of 95% air and 5% CO_2 at a temperature of 37 °C. To continue the culture, the cells were collected using a trypsin-EDTA solution twice a week and then seeded into dishes at a density of 10^6 cells per dish. For the purpose of experimentation, cells from the eighth and twentieth passages were utilized.

2.4 In vitro cell viability assay

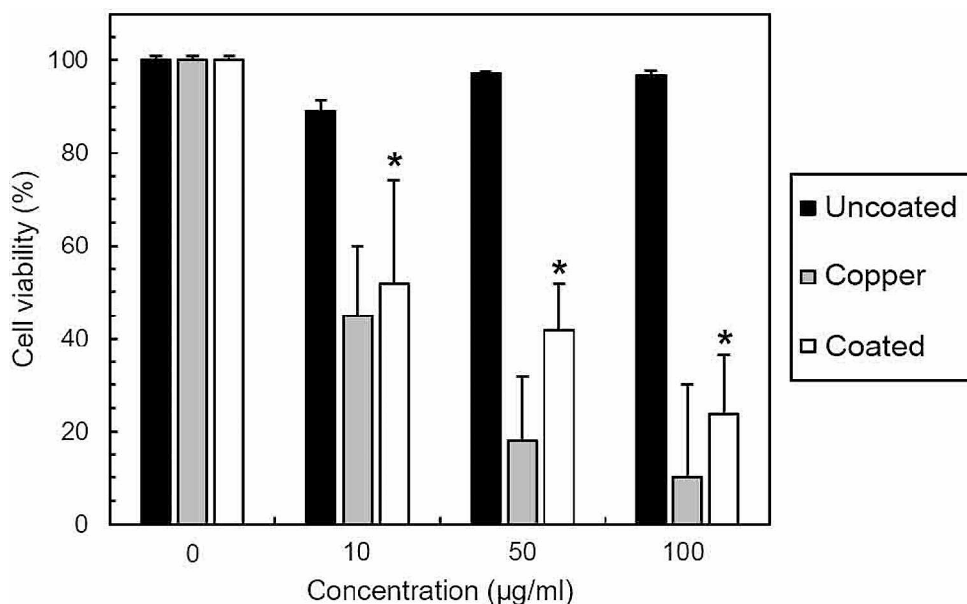
C6 glioma cells, initially seeded at a density of 30,000 cells per well, were cultivated in 96-well plates under standard culture conditions. The cells were treated for 8 h with different concentrations (10, 50 and 100 $\mu\text{g/mL}$) of bionanocatalysts and coated bionanocatalysts diluted in serum free DMEM. Twenty-four hours prior to exposure, the culture medium was replaced with fresh serum-free medium. To assess cell viability and mitochondrial function, we employed the 3-(4,5-dimethyl-2-thiazolyl)-2,5-diphenyl-2 H-tetrazolium bromide (MTT) assay, which measures the reduction of MTT to MTT-formazan by cellular mitochondrial dehydrogenases. After exposure to orexin A and

orexin B for 24 and 48 h, the cell cultures were rinsed with PBS before adding MTT (0.5 mg/ml). The cells were then incubated for 3 h at 37 °C. The formazan crystals were dissolved in 100% dimethyl sulfoxide (DMSO), and the absorbance, which is proportional to the number of viable cells, was assessed at 570 nm using a microplate reader (EnVision 2103, PerkinElmer). The mean inhibitory concentration (IC₅₀) was calculated by calculating the four-parameter dose-response curve.

2.5 Immunocytochemistry and microscopy

For double labeling immunofluorescence, the cells were fixed with 2% paraformaldehyde in phosphate buffer (PBS) at room temperature (RT) for 15 min and permeated in 0.1% Triton X-100-PBS (PBS/T). After blocking for 1 h at RT (0.5% gelatin and 1.5% fetal bovine serum in PBS), cells were incubated for 1 h. at RT in a humidity chamber with antibody anti- α -tubulin monoclonal-IgG (Santacruz Biotechnology, TX, USA). The corresponding secondary antibodies to mouse-IgG were tagged with fluorescein-isothiocyanate (FITC, Jackson ImmunoResearch Labs, PA, USA), and incubated in PBS/T for 1 h at RT (1:1000 dilution). The actin cytoskeleton was stained with dye Rhodamine-Phalloidin (Invitrogen, NY, USA). In experiments with cells, in vivo labeling was done by including the fluorescent mitochondrial marker MitroTracker Deep Red (Invitrogen). Immunolabeled cells were analyzed by epifluorescence through 60x (numerical aperture (NA):1.00 W) and a 100x (NA: 1.3 Oil) Plan-Fluor Lens coupled to a Nikon Eclipse-80i Microscope (Nikon Corp, Tokyo, Japan). The images were obtained and recorded by using a Nikon digital sight-DG-Ri1 camera controlled with the Nikon NIS-Elements AR-3.0- SP7 software included in the system (Nikon Corp).

Fig. 1 Catalytic cytotoxic effect of bionanocatalysts as a function of cell viability at different concentrations and comparison against pure copper cytotoxicity. Significant differences (*) were determined as $p < 0.05$



2.6 Statistical analysis

All data are presented as the mean \pm standard error of the mean and 95% confidence interval. Statistical tests and biological replicates are indicated in the figure captions. All statistical analyses were performed with GraphPad Prism v8.0 software. An alpha level of $p < 0.05$ was set as the threshold for significance.

3 Results and discussion

3.1 Cytotoxicity through bionanocatalytic activity

The cytotoxic effect in terms of cell viability of glioma C6 cells treated with different concentrations of bionanocatalysts is shown in Fig. 1. As can be seen, the mixed oxide catalytic matrix does not generate a significant decrease in the percentage of cell viability with respect to untreated cells. In contrast, the copper-coated bionanocatalyst generated a significant shift in the number of viable cells from the concentration of 10 μ g/mL. This phenomenon suggests a high intrinsic biocompatibility of the oxide matrix by not exerting considerable cell death, while the coating with copper groups considerably increases the cytotoxic activity of the bionanocatalyst. Pure copper cytotoxicity evaluation is included as a control. The cytotoxicity of copper-coated nanocomposites is widely known [15], its main mechanisms of action being DNA damage through catalytic formation of reactive oxygen species [46]. In previous work, we have demonstrated the high dispersion of copper-coating nanostructured agents in oxide matrices [11, 27, 28]. As in the present work, the coating with the cuprous derivatives gave the bionanocatalysts enhanced antineoplastic properties. In

particular, these copper-coated bionanocatalysts were found to exert part of their cytotoxic activity due to the catalytic degradation of the DNA [22].

3.2 Mechanisms of cytotoxicity

To delve deeper into these mechanisms, we examined cell morphology following the introduction of bionanocatalysts. In Fig. 2, we present an analysis of C6 glioma cell cytoskeleton interactions with copper-coated bionanocatalysts. In the brightfield images, we can discern the presence of crystals formed due to the aggregation of these nanostructures. Notably, in cells treated with the matrix the radial arrangement of the tubulin cytoskeleton (identified through anti- α -tubulin staining in the green channel) and the fibrillar actin structure (revealed via rhodamine-phalloidin staining in the red channel, white arrows) both maintain their normal and unaffected structure. In contrast, the coated bionanocatalysts lead to the disruption of the central microtubule structure, transforming it into a structure that encircles the nucleus. Consequently, this transformation results in the complete degradation of actin filaments, as indicated by the arrowheads. This outcome unequivocally demonstrates that the presence of copper coating in the matrix induces a significant alteration in the cytoskeletal structure. Previous

studies suggest that such destabilization may take place through a catalytic proteolysis, in which the bionanocatalyst act as a cleavage compound for the carbon-carbon and carbon-nitrogen bonds within the cytoskeleton protein [34, 43].

Finally, to corroborate the impact of the catalytic activity of bionanocatalysts on the metabolic activity of mitochondria in C6 cells, staining by MitoTracker Deep Red dye was performed to identify metabolically active mitochondria (Fig. 3). Under control conditions (uncoated matrix), we observed the typical morphology of the organelles. However, in cells exposed to the coated bionanocatalysts, the mitochondrial network underwent significant structural modifications. The bionanocatalysts accumulated around the nucleus, causing the mitochondria to lose their normal network-like structure. Additionally, these cells displayed an elongated morphology distinct from the majority of fibers. Recent studies have firmly established that changes in the morphology of mitochondria indicate the onset of stress, shifts in the redox state, and the initiation of apoptosis [1]. Consequently, our results clearly indicate a significant cytotoxicity and pronounced distortions in mitochondrial morphology.

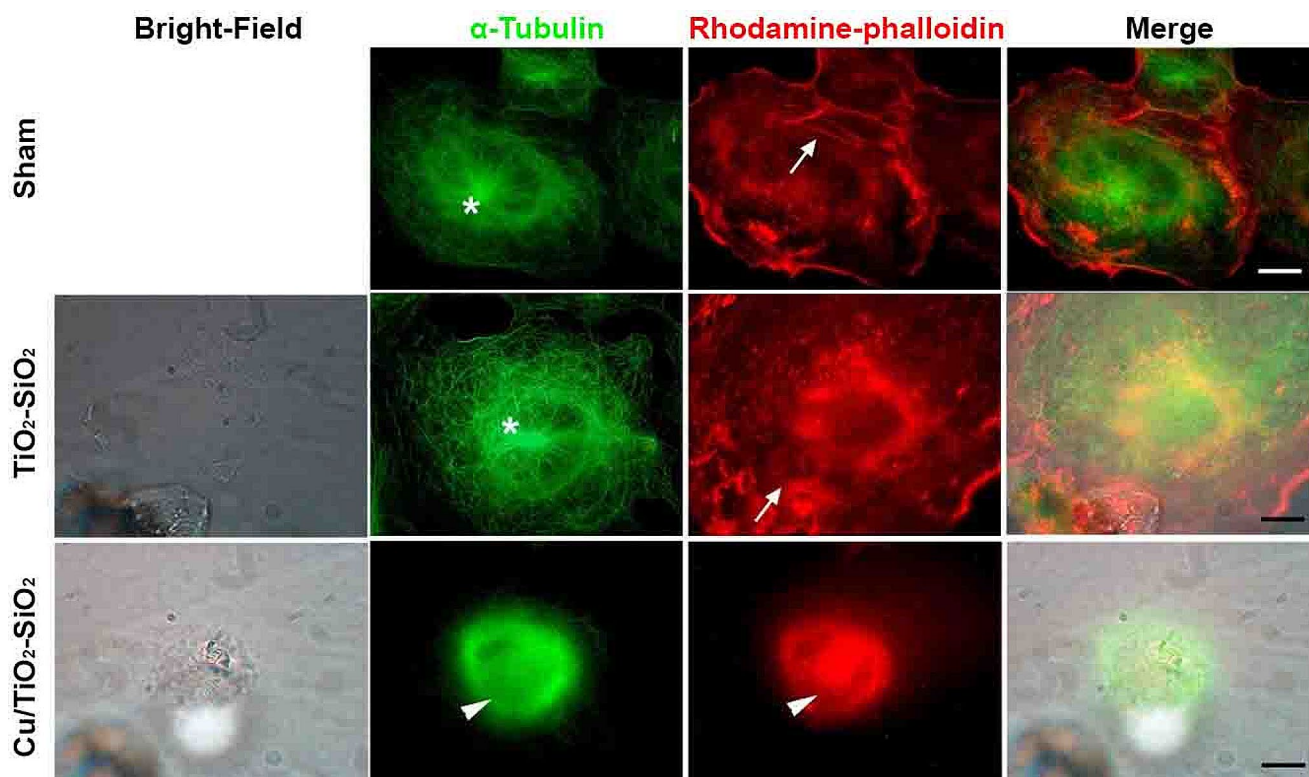
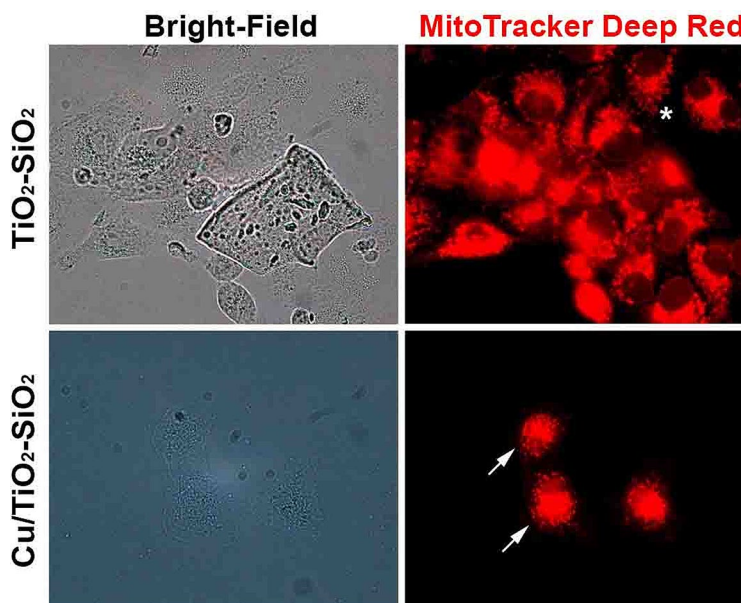


Fig. 2 Cytoskeleton integrity evaluation by double-labelling with α -tubulin and rhodamine-phalloidin showing organelle disorganization as a function of bionanocatalysts activity. The nucleus is indicated with

an asterisk (*). Arrows indicate normal cytoskeleton, whereas arrowheads indicate filament degradation

Fig. 3 Mitochondrial network integrity evaluation by MitoTracker Deep Red showing damage due to bionanocatalyst concentration in the surrounding nucleus



3.3 Bionanocatalyst atomic composition

To further understand the cytotoxic capacity of the bionanocatalysts, a physicochemical characterization was carried out. Figure 4a shows the XPS patterns of the two bionanocatalysts evaluated. The high-resolution XPS spectra for each component are shown in Fig. 4b-f. The deconvolution of the Cu 2p region reveals several key signals. The primary peak, situated at 934.05 eV, is attributed to the Cu 2p_{3/2} state of Cu²⁺ within cupric oxide (CuO) [53]. Its accompanying Cu 2p_{1/2} signal is found at a 20.0 eV split, which is characteristic of copper oxides and lies in the same spectral region [5]. Additionally, though less pronounced in intensity, another component emerges at 932.57 eV (with a corresponding 20.0 eV counterpart), potentially associated with either Cu⁺ in Cu₂O or Cu⁰ [18]. Unhappily, through XPS analysis it is not possible to discern between these two states [18].

These various oxidation states of copper play a crucial role in achieving a catalytic enhancement effect [8]. This effect arises from the overlapping of the conduction bands of the oxide matrix, leading to increased catalytic activity [6]. In the case of TiO₂, this phenomenon results in a shift in its photocatalytic activity from ultraviolet to visible light [16]. Furthermore, three signals, each with a complementary component at approximately 20.0 eV, are observable at 939.37, 942.26, and 944.39 eV. The first of these signals can be attributed to Cu(OH)₂ [18], likely corresponding to surface copper-coating nanoparticles stabilized by hydrogen interactions with the matrix. The second signal has not been classified in the literature and may represent a unique bond formed between Cu and the oxide matrix, possibly through

coordination bonds [50]. The last signal corresponds to a satellite feature associated with the Cu²⁺ signal [16].

Regarding the catalytic oxide matrix, the signal deconvolution for Si 2p (Fig. 4c) indicates the presence of different oxidation states: Si⁺ (suboxides SiO_x), Si⁴⁺ (silicon dioxide, SiO₂), and Si³⁺ (Si-O-Si bond) [14, 37, 38], the latter being the preponderant one in the bionanocatalyst matrix. No signals were observed for Si⁰ or Si²⁺, indicating that all Si in the bionanocatalyst matrix is oxidized and that no organic remnants are directly bound to Si, respectively [38, 55]. In the other hand, Fig. 4d shows the de-convolution of XPS spectra for Ti 2p. The peaks observed at 458.68 and 464.38 eV correspond to the Ti⁴⁺ 2p_{3/2} and Ti⁴⁺ 2p_{1/2}, respectively. The shoulder peaks at 459.81 and 465.51 eV represent traces of Ti³⁺ 2p_{3/2} and Ti³⁺ 2p_{1/2}. The binding energy difference (Δ) for (Ti⁴⁺ 2p_{3/2} - Ti⁴⁺ 2p_{1/2}) and (Ti³⁺ 2p_{3/2} - Ti³⁺ 2p_{1/2}) is 5.7 for both, which is similar to the reported by previous study [30]. The Ti³⁺ state is known to be presented due to oxygen deficiency and high hydrogen concentration in the network [40]. In this regard, in the O 1s region (Fig. 4e), both samples exhibit two signals: one attributed to the Si-O bonding [36], and the other attributed to oxygen vacancies [41]. Bi et al. [3] observed that TiO₂ exhibits high visible light response and stable photocatalytic activity owing to the presence of rich oxygen vacancies and Ti³⁺, which act as traps to reduce the recombination of e⁻/h⁺ pairs, hence potentiating the catalytic activity of the oxide.

Finally, regarding the C 1s region, Fig. 4f shows four signals: the first two correspond to the C-C bond, which exhibits a sp² hybridization state (attributable to the delocalized electrons in the acetylacetonate group), and a sp³ hybridization state (attributable to organic remnants generated during the hydrolysis process of the precursor alkoxide in the

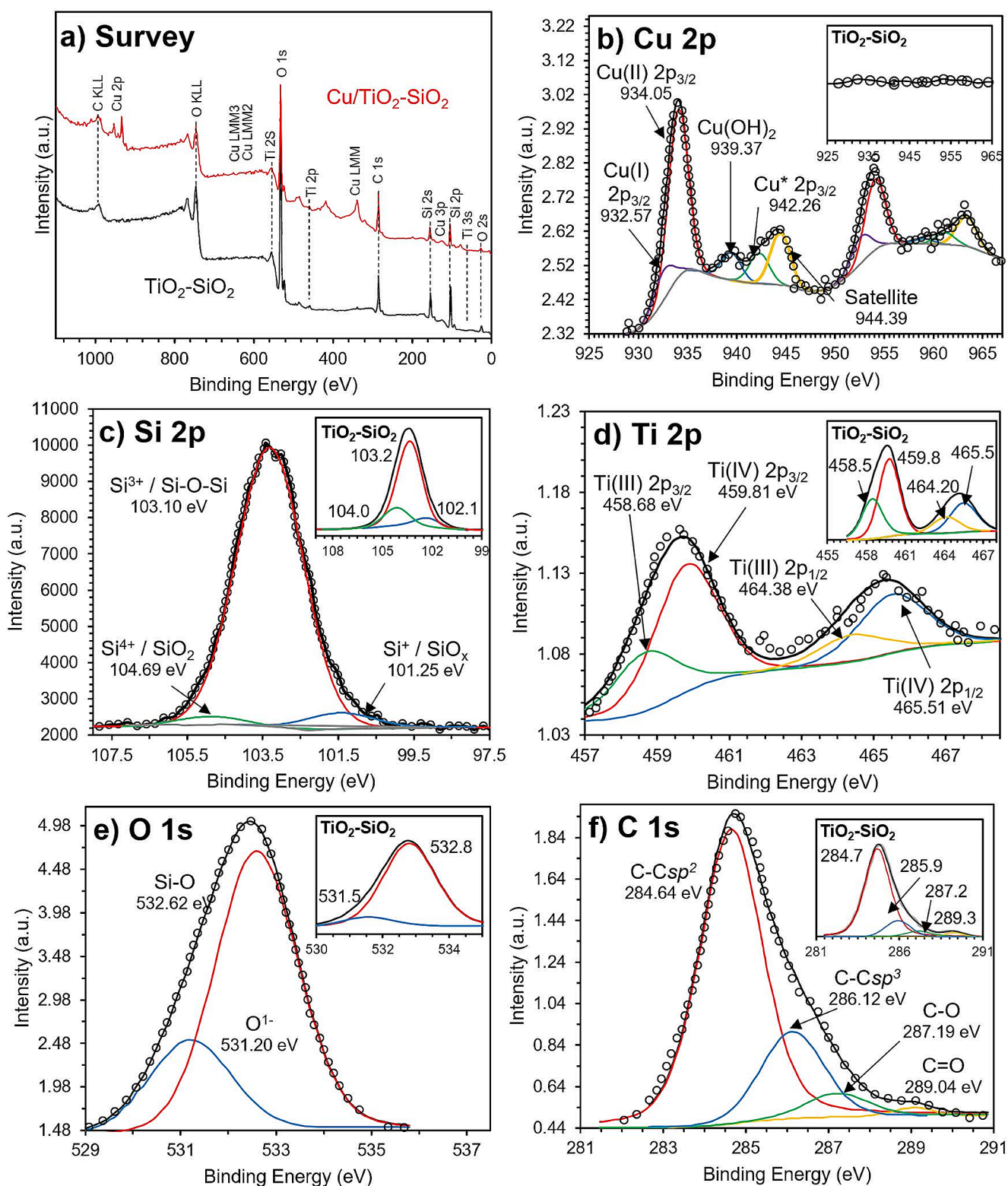


Fig. 4 (a) XPS and (b-f) high-resolution XPS spectra of coated bionanocatalysts compared to uncoated bionanocatalyst showing peaks for (b) Cu 2p, (c) Si 2p, (d) Ti 2p, (e) O 1s, and (f) C 1s

synthesis) [36]. The other additional signal corresponds to the C-O bond which is associated with the OH groups of the acetylacetonate group [12]. It is to be noted that the corroboration of the presence of all the bond signals attributed to the acetylacetonate group confirms the presence of the group. It has been found that this molecule is essential during the coating of the matrix so as to achieve high dispersion of copper. Finally, the last signal corresponds to ambient CO₂ deposited on the surface of the bionanocatalyst [38].

3.4 Bionanocatalyst morphology and particle size

The morphology of bionanocatalysts is observed by SEM and TEM (Fig. 5). Coated bionanocatalysts are observed to form smooth and amorphous clusters with sizes on the order of 500 nm (see Fig. 5a). In contrast, transmission electron microscopy (TEM) analysis of the coated bionanocatalysts reveals crystalline structures (Fig. 5b) and particle sizes around 10 nm (Fig. 5c). The SAED patterns of copper-coated bionanocatalysts (Fig. 5d) in rutile phase exhibit scattered ring patterns devoid of extra diffraction spots and rings from secondary phases, indicating their strong crystalline structure.

For the uncoated matrix, SEM imaging (Fig. 5e) shows the formation of conglomerates with diameters around 200 nm. These conglomerates are spherical and have a smooth surface. TEM examination of individual particles confirms their crystallinity (Fig. 5f) and sizes to be approximately 10 nm (Fig. 5g). It is worth noting that the high

dispersion and low concentration of coating copper in the coated sample seems to alter the conglomerate structure of the bionanocatalysts: the SAED patterns of oxide matrix (Fig. 5h) shows that the brightness and intensity of polymorphic ring is weak, so they are poorly crystallized and partly amorphous; however, the structure and size of the individual nanoparticle remains the same (Fig. 5c and g).

3.5 Bionanocatalyst surface properties

Figure 6a illustrates the FTIR spectra (2000–400 cm⁻¹) of coated and uncoated bionanocatalysts and the copper precursor used. In the titanosilicate spectrum, a peak is observed around 1629 cm⁻¹, which is attributed to the bending vibration of the O-H bond, indicative of adsorbed water molecules. Additionally, peaks at 796 and 1086 cm⁻¹ are attributed to the symmetric and asymmetric stretching vibrations of Si-O-Si bonds, respectively [42]. The peak at 944 cm⁻¹ corresponds to the Ti-O-Si asymmetric stretching vibration, confirming the formation of Ti-O-Si linkages [42]. This suggests the replacement of some silicon atoms in the silica network by titanium atoms, resulting in the titanosilicate mixed oxide. Regarding the Cu(acac)₂ spectra, peaks at 1577, 1555, and 1533 cm⁻¹ correspond to C=C and C=O stretching vibrations, while the peak at 684 cm⁻¹ is attributed to Cu-O stretching vibrations between the copper-coating atom and the oxygen atoms in the acetylacetonate ions [47]. The 610 cm⁻¹ peak is due to ring vibrations and Cu-O stretching vibration modes, and the peaks at 451 cm⁻¹ and

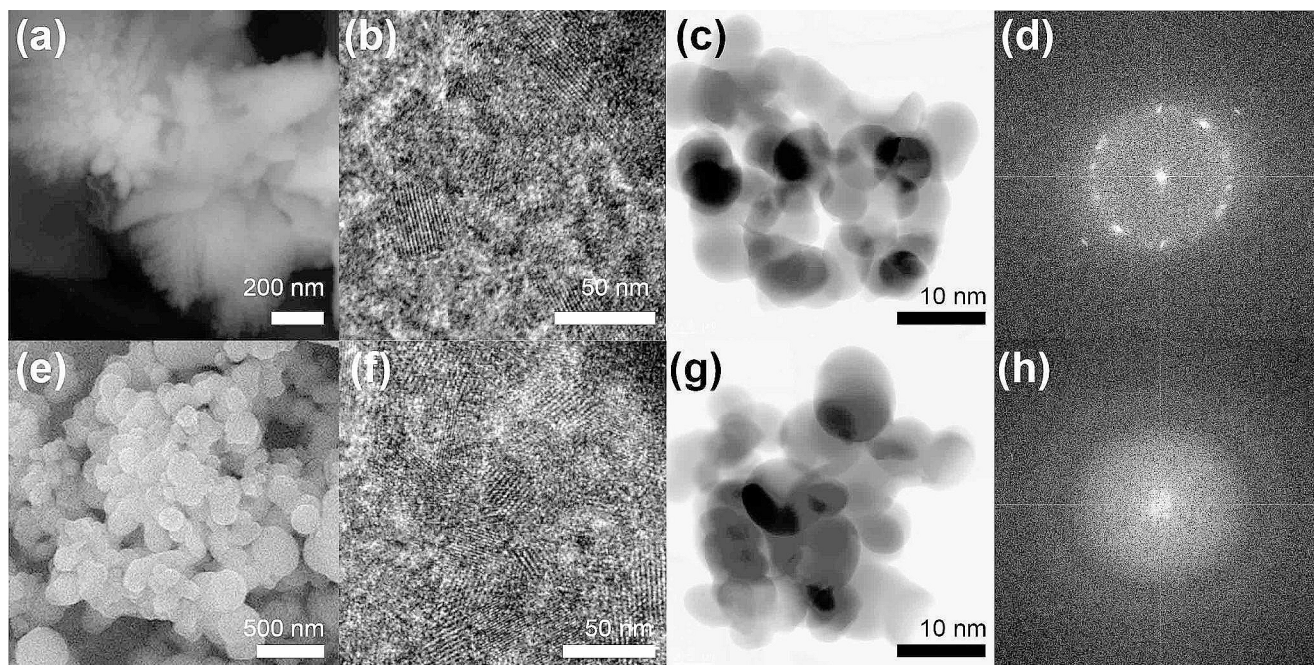


Fig. 5 (a, e) SEM, (b, f) TEM, (c, g) high-resolution TEM micrographs, and SAED (d, h) of the compounds (a-d) coated and (e-h) uncoated bionanocatalysts

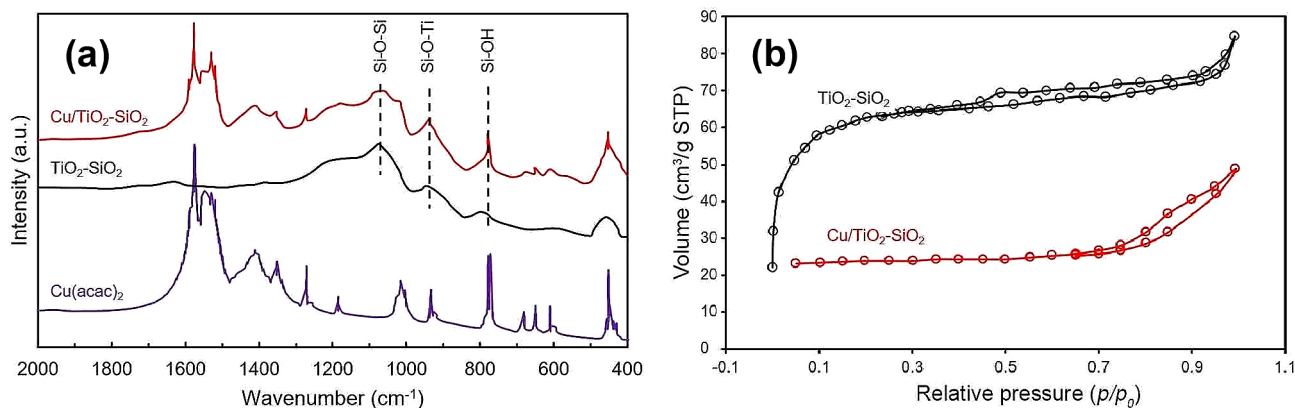


Fig. 6 (a) FTIR spectra of coated and uncoated bionanocatalysts, as well as copper precursor $\text{Cu}(\text{acac})_2$. (b) BET isotherms of coated and uncoated bionanocatalysts

Table 1 Textural properties of the bionanocatalysts

Bionanocatalyst	BET surface area (m^2/g)	Mesopore volume (cm^3/g)	Average pore size (nm)
TiSiO_x	320	0.423	5.28
Cu/TiSiO_x	61	0.200	3.28

431 cm^{-1} are related to Cu-O and ring deformation modes. Upon analyzing the coated bionanocatalysts spectrum, several similarities with the uncoated and $\text{Cu}(\text{acac})_2$ spectra were found, confirming the presence of characteristics from both $\text{Cu}(\text{acac})_2$ and TiSiO_x .

Surface area, pore volume, and pore diameter data (Table 1) were obtained using the BET and BJH methods based on nitrogen adsorption-desorption isotherms (Fig. 6b). The uncoated sample exhibits a surface area of $320\text{ m}^2/\text{g}$, a pore volume of $0.423\text{ cm}^3/\text{g}$, and a pore diameter of 5.28 nm . Interestingly, the sample coated with copper exhibited a significant reduction in these values, especially in terms of BET surface area. This decline suggests that the copper-coating complexes modify the mesoporous structure of the matrix upon coating, as it is known that such nanoparticles fill the pores of the oxide matrix [9]. It is to be noted, however, that such a decrease in surface area does not exert a negative effect on the reactivity of the material, but, on the contrary, increases the cytotoxic activity of the nanostructures as evidenced in Fig. 1. This is due to the very nature of bionanocatalysts as catalytic ultra-nanoparticles with colloid-like behavior [21]. In normal catalysts, the surface area is directly related to the reactivity of the material. However, in ultra-nanoparticulate bionanocatalysts, their reactivity is directly linked to the metallic agents with which their surface is coated, to their overall size of 1 to 3 nm, and to the surface functionalizing agents.

3.6 Bionanocatalysts' mechanisms of action in terms of structural composition

As a whole, the physicochemical characterization suggests that the bionanocatalysts are composed of a mixed matrix of titanosilicate in which copper-coating nanoparticles (mainly CuO) are homogeneously dispersed in the surface of the matrix and determine the morphological and textural properties of the bionanocatalyst clusters (without affecting the structure of the individual nanoparticles), as well as the catalytic activity of the nanostructures by overlapping the conduction bands of the matrix oxides. In turn, copper-coating nanoparticles endow the intrinsically biocompatible titanosilicate matrix with an antineoplastic capacity by allowing it to exert cytotoxic activity on the genetic material of cancer cells, destabilize the cytoskeleton and, finally, alter the oxide-reductive activity of mitochondria, leading them to the activation of programmed cell death by apoptosis.

In previous work we have demonstrated the high selectivity of this type of bionanocatalysts for exclusive cancer cells, without affecting normal cells *in vitro* [11]. Similarly, other studies have examined the function of the oxide matrix as a cytotoxic chemical buffering agent in healthy cells at the cellular level. For instance, Lopez et al. discovered that the nanostructured TiO_2 matrix reduced the phototoxic effects of zinc phthalocyanine by up to 80% compared to the pure substance by restricting the drug's entry into healthy cells [25]. Similarly, studies have shown that the functionalized matrix of onco-bionanocatalysts lacking transition metals does not harm cells, as evidenced by various cell viability tests [24, 26, 28]. This has also been confirmed by several clinical studies performed on chronic wounds where this type of bionanocatalysts composed of TiO_2 , SiO_2 and superficial CuO were used as disinfectant agents in open wounds, without any observable side effects or damage to the surrounding healthy tissues for up to 6 months [29, 30]. An intriguing correlation exists between the surface coating

and natural biocompatibility of the nanostructured matrix of bionanocatalysts [2]. These findings underscore the biosafety of bionanocatalysts. However, further investigation across various cell lines and tissues is necessary to fully elucidate their selective toxicity and biocompatibility.

In addition, we have proposed hypotheses related to the possible mechanisms of action of this type of nanostructures for the selective bionanocatalytic cleavage of carbon-carbon and carbon-nitrogen bonds in the genetic material of cancer cells [31]. In this regard, in a previous work, the kinetics of degradation of genetic material in C6 glioma cells guided by the formation of adducts from the first 30 min of interaction was evaluated [23]. Remarkably, after the first 60 min of incubation, the genetic material had been completely degraded, demonstrating enhanced activity with respect to cisplatin whose genotoxic potential was observed up to 180 min. However, considering the other two mechanisms of action of bionanocatalysts for the elimination of cancer cells, it is necessary to deepen our understanding of their cytotoxicity kinetics. Although in the present work a significant increase in cell death was observed after 8 h of interaction, future work should evaluate the rate of cell viability as a function of time, so that the time of action of the nanostructures can be known.

When bionanocatalysts interact with DNA, they induce the breaking of bonds throughout the genetic material at a rapid rate. This damage occurs randomly across the DNA structure, overwhelming repair mechanisms. In line with current understanding, if DNA repair mechanisms fail, cells activate programmed cell death pathways, such as apoptosis [13]. Essentially, cells in a tissue that sustain DNA damage beyond repair capacity are eliminated from the population. DNA damage often triggers death receptors outside the cell

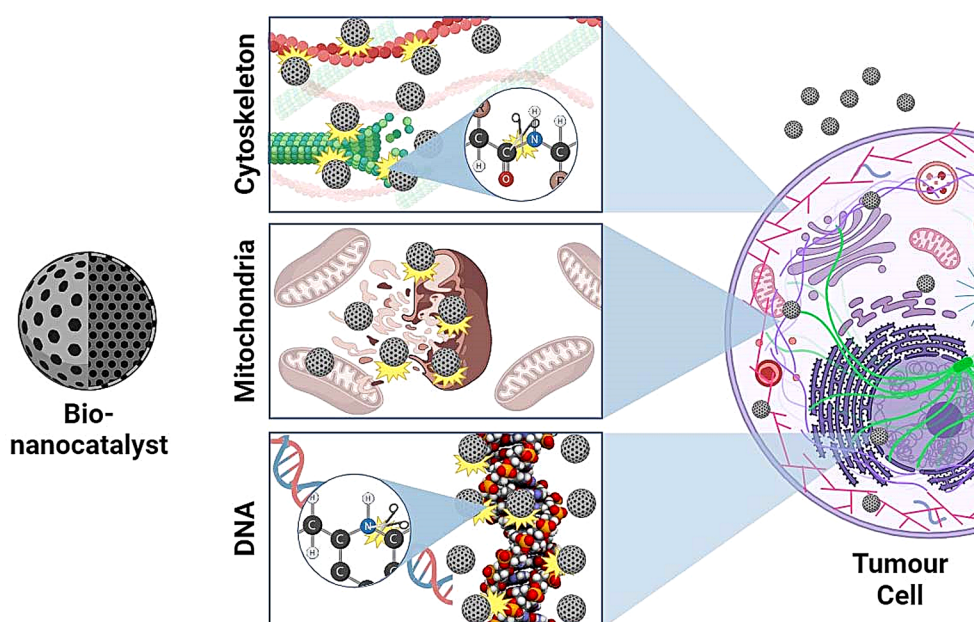
(such as Fas, CD95, Apo-1) and/or internal mitochondrial apoptotic pathways [7]. The Fas signaling pathway involves receptor activation, formation of the DIS complex (consisting of FADD, Fas-associated protein with a death domain, and procaspase-8 and –10), and initiation of the caspase cascade, leading to DNA cleavage by CAD (caspase-activated DNAase) and degradation of intracellular proteins by caspase-3 and –7 [54]. Conversely, the mitochondrial apoptotic pathway revolves around the regulation of cytochrome c release from mitochondria into the cytoplasm, along with proapoptotic proteins like Bax and Bak, countered by anti-apoptotic proteins like Bcl-2 and Bcl-XL. Upon cytochrome c release, apoptosomes containing procaspase-9, Apaf-1, and cytochrome c assemble, initiating the caspase cascade, ultimately leading to protein and DNA breakdown [51].

In this sense, the present work deepens in the cytotoxic mechanisms of bionanocatalysts and evidences the possibility of using copper-coating nanoparticles (in contrast with previous findings using silver and platinum nanoparticles [23, 32]); for the potentiation of the matrix. The above is summarized in Fig. 7.

4 Conclusions

In the present work, the cytotoxic activity towards glioma cancer cells of a new type of bionanocatalysts based on a catalytic mixed oxide matrix, in which copper-coating nanoparticles were homogeneously dispersed on its surface for the optimization of the intrinsic catalytic properties of the matrix and the generation of cytotoxic properties, was evaluated. Copper-coated bionanocatalysts were able to significantly reduce cell viability compared to reference

Fig. 7 Cytotoxic mechanisms of action of bionanocatalysts: destabilization of cytoskeleton, mitochondria, and DNA through bond cleavage



bionanocatalysts. Structural damage to the cytoskeleton and mitochondrial activity were observed, suggesting these pathways as part of the mechanisms of action of these nanostructures derived from their bionanocatalytic activity for bond breaking. The physicochemical studies corroborated that the functionalization with copper-coating species (mainly CuO) did not alter the individual structure of the bionanocatalysts but enhanced their cytotoxic activity. With this work, it is expected to deepen in the mechanisms of action of this potential antineoplastic treatment and to evidence the use of copper-coating nanoparticles as potentiating agents of the intrinsic properties of the bionanocatalysts.

Acknowledgements None to be declared.

Author contributions All authors contributed equally. The manuscript was written through contributions of all authors. All authors have given approval to the final version of the manuscript.

Funding Open access funding provided by Universidad Autonoma Metropolitana (BIDIUAM). The authors received no funding for the development of the article.

Open access funding provided by Universidad Autonoma Metropolitana (BIDIUAM)

Data availability The raw/processed data can be shared at adequate request.

Declarations

Ethical approval It is not applicable.

Competing interest The authors declare that they have no known competing financial interests or personal relationships that could have appeared to influence the work reported in this paper.

Open Access This article is licensed under a Creative Commons Attribution 4.0 International License, which permits use, sharing, adaptation, distribution and reproduction in any medium or format, as long as you give appropriate credit to the original author(s) and the source, provide a link to the Creative Commons licence, and indicate if changes were made. The images or other third party material in this article are included in the article's Creative Commons licence, unless indicated otherwise in a credit line to the material. If material is not included in the article's Creative Commons licence and your intended use is not permitted by statutory regulation or exceeds the permitted use, you will need to obtain permission directly from the copyright holder. To view a copy of this licence, visit <http://creativecommons.org/licenses/by/4.0/>.

References

- Abate, M., Festa, A., Falco, M., Lombardi, A., Luce, A., Grimaldi, A., Zappavigna, S., Sperlongano, P., Irace, C., Caraglia, M., Misso, G.: Mitochondria as playmakers of apoptosis, autophagy and senescence. *Semin Cell. Dev. Biol.* **98**, 139–153 (2020). <https://doi.org/10.1016/j.semcdb.2019.05.022>
- Alvarez Lemus, M.A., Monroy, H., López, T., De la Cruz Hernández, E.N., López-González, R.: Effect of surface modification on the bioactivity of sol-gel TiO₂-based nanomaterials. *J. Chem. Technol. Biotechnol.* **91**, 2148–2155 (2016). <https://doi.org/10.1002/jctb.4915>
- Bi, X., Du, G., Kalam, A., Sun, D., Yu, Y., Su, Q., Xu, B., Al-Sehemi, A.G.: Tuning oxygen vacancy content in TiO₂ nanoparticles to enhance the photocatalytic performance. *Chem. Eng. Sci.* **234**, 116440 (2021). <https://doi.org/10.1016/j.ces.2021.116440>
- Bokhimi, X., Novaro, O.O., Gonzalez, R.D., López, T., Chimal, O., Asomoza, A., Gómez, R.: Copper Precursor Effect on Reducibility and Titania Concentration of Sol-Gel Cu/TiO₂ Catalyst. *J. Solid State Chem.* **144**, 349–353 (1999). <https://doi.org/10.1006/jssc.1999.8164>
- Briggs, D.: Handbook of X-ray Photoelectron Spectroscopy C. D. Wanger, W. M. Riggs, L. E. Davis, J. F. Moulder and G. E. Muilenberg Perkin-Elmer Corp., Physical Electronics Division, Eden Prairie, Minnesota, USA, 1979. 190 pp. \$195. Surface and Interface Analysis. 3, v–v (1981). <https://doi.org/10.1002/sia.740030412>
- Dasireddy, V.D.B.C., Likozar, B.: The role of copper oxidation state in Cu/ZnO/Al₂O₃ catalysts in CO₂ hydrogenation and methanol productivity. *Renew. Energy.* **140**, 452–460 (2019). <https://doi.org/10.1016/j.renene.2019.03.073>
- Fas, S.C., Fritzsching, B., Suri-Payer, E., Krammer, P.H.: Death receptor signaling and its function in the Immune System. In: Apoptosis and Its Relevance to Autoimmunity, pp. 1–17. KARGER, Basel (2005)
- Fridman, V.Z., Davydov, A.A.: Dehydrogenation of Cyclohexanol on copper-containing catalysts. *J. Catal.* **195**, 20–30 (2000). <https://doi.org/10.1006/jcat.2000.2979>
- Gołabiewska, A., Lisowski, W., Jarek, M., Nowaczyk, G., Michalska, M., Jurga, S., Zaleska-Medynska, A.: The effect of metals content on the photocatalytic activity of TiO₂ modified by Pt/Au bimetallic nanoparticles prepared by sol-gel method. *Mol. Catal.* **442**, 154–163 (2017). <https://doi.org/10.1016/j.mcat.2017.09.004>
- Gomez, R., Lopez, T., Herrera, L., Castro, A.A., Scelza, O., Baronetti, G., Lazzari, E., Cuan, A., Campos, M., Poulain, E., Ramirez-Solis, A., Novaro, O.: Oxidative coupling of Methane over Sol-Gel Magnesium Oxide catalysts: Effect on selectivity to olefin formation. *Stud. Surf. Sci. Catal.* **75**, 2213–2216 (1993). [https://doi.org/10.1016/S0167-2991\(08\)64263-9](https://doi.org/10.1016/S0167-2991(08)64263-9)
- González-Larraz, P.G., López-Goerne, T.M., Padilla-Godínez, F.J., González-López, M.A., Hamdan-Partida, A., Gómez, E.: IC50 Evaluation of platinum nanocatalysts for Cancer treatment in fibroblast, HeLa, and DU-145 cell lines. *ACS Omega.* **5**, 25381–25389 (2020). <https://doi.org/10.1021/acso.omega.0c03759>
- Gustus, R., Gruber, W., Wegewitz, L., Geckle, U., Prang, R., Kübel, C., Schmidt, H., Maus-Friedrichs, W.: Decomposition of amorphous Si₂C by thermal annealing. *Thin Solid Films.* **552**, 232–240 (2014). <https://doi.org/10.1016/j.tsf.2013.12.033>
- Hakem, R.: DNA-damage repair; the good, the bad, and the ugly. *EMBO J.* **27**, 589–605 (2008). <https://doi.org/10.1038/emboj.2008.15>
- Himpfel, F.J., McFeely, F.R., Taleb-Ibrahimi, A., Yarmoff, J.A., Hollinger, G.: Microscopic structure of the SiO₂/Si interface. *Phys. Rev. B.* **38**, 6084–6096 (1988). <https://doi.org/10.1103/PhysRevB.38.6084>
- Ingle, A.P., Duran, N., Rai, M.: Bioactivity, mechanism of action, and cytotoxicity of copper-based nanoparticles: A review. *Appl. Microbiol. Biotechnol.* **98**, 1001–1009 (2014). <https://doi.org/10.1007/s00253-013-5422-8>
- Janczarek, M., Kowalska, E.: On the origin of enhanced photocatalytic activity of copper-modified Titania in the oxidative reaction systems. *Catalysts.* **7**(317) (2017). <https://doi.org/10.3390/catal7110317>
- Janczarek, M., Kowalska, E.: On the origin of enhanced photocatalytic activity of copper-modified Titania in the

- oxidative reaction systems. *Catalysts*. **7**(317) (2017). <https://doi.org/10.3390/catal7110317>
- 18 Karimzadeh, M., Niknam, K., Manouchehri, N., Tarokh, D.: A green route for the cross-coupling of azide anions with aryl halides under both base and ligand-free conditions: Exceptional performance of a Cu₂O–CuO–Cu–C nanocomposite. *RSC Adv.* **8**, 25785–25793 (2018). <https://doi.org/10.1039/C8RA04608E>
 - 19 López Goerne, T.M.: *Nanotecnología Y Nanomedicina: La Ciencia Del futuro... hoy*. Arkhé Ediciones, Ciudad de México (2011)
 - 20 López Goerne, T.M.: *Nanomedicina catalítica: ciencia y cáncer*. Arkhé Ediciones, Ciudad de México (2013)
 - 21 López, T., Bosch, P., Tzompantzi, F., Gómez, R., Navarrete, J., López-Salinas, E., Llanos, M.E.: Effect of sulfation methods on TiO₂–SiO₂ sol–gel catalyst acidity. *Appl. Catal. Gen.* **197**, 107–117 (2000). [https://doi.org/10.1016/S0926-860X\(99\)00541-4](https://doi.org/10.1016/S0926-860X(99)00541-4)
 - 22 López, T., Cuevas, J.L., Ilharco, L., Ramírez, P., Rodríguez Reinoso, F., Rodríguez-Castelleón, E.: XPS characterization and E. Coli DNA degradation using functionalized Cu/TiO₂ nanobiocatalysts. *Mol. Catal.* **449**, 52–71 (2018). <https://doi.org/10.1016/j.mcat.2018.02.010>
 - 23 López, T., Figueras, F., Manjarrez, J., Bustos, J., Alvarez, M., Silvestre-Albero, J., Rodríguez-Reinoso, F., Martínez-Ferre, F., Martínez, E.: Catalytic nanomedicine: a new field in antitumor treatment using supported platinum nanoparticles. In vitro DNA degradation and in vivo tests with C6 animal model on Wistar rats. *Eur J Med Chem.* **45**, 1982–1990. (2010). <https://doi.org/10.1016/J.EJMECH.2010.01.043>
 - 24 López, T., Ortiz, E., Alvarez, M., Manjarrez, J., Montes, M., Navarro, P., Odriozola, J.A.: Catalytic nanomedicine: Functionalisation of nanostructured cryptomelan. *Mater Chem Phys.* **120**, 518–525. (2010). <https://doi.org/10.1016/J.MATCHEMPHYS.2009.11.049>
 - 25 Lopez, T., Ortiz, E., Alvarez, M., Navarrete, J., Odriozola, J.A., Martinez-Ortega, F., Páez-Mozo, E., Escobar, P., Espinoza, K.A., Rivero, I.A.: Study of the stabilization of zinc phthalocyanine in sol-gel TiO₂ for photodynamic therapy applications. *Nanomedicine.* **6**, 777–785 (2010). <https://doi.org/10.1016/j.nano.2010.04.007>
 - 26 López, T., Ortiz, E., Guevara, P., Gómez, E., Novaro, O.: Physicochemical characterization of functionalized-nanostructured-titania as a carrier of copper complexes for cancer treatment. *Mater. Chem. Phys.* **146**, 37–49 (2014). <https://doi.org/10.1016/j.matchemphys.2014.02.039>
 - 27 López, T., Ortiz-Islas, E., Guevara, P., Rios, J.V.: Preparation and characterization of copper compounds co-gelled with nanostructured TiO₂ materials to be used in cancer treatment. *Sci. Adv. Mater.* **4**, 579–583 (2012). <https://doi.org/10.1166/SAM.2012.1322>
 - 28 López, T., Ortiz-Islas, E., Guevara, P., Rodríguez-Reinoso, F., Gómez, E., Cuevas, J.L., Novaro, O.: Release of copper complexes from a nanostructured sol–gel titania for cancer treatment. *J. Mater. Sci.* **50**, 2410–2421 (2015). <https://doi.org/10.1007/S10853-014-8796-9>
 - 29 López, T., de la Barquera, S., Padilla-Godínez, V., Ramírez, F.J., Gómez-López, P., E.: Post-breast Cancer Chronic wounds with Solid calcifications treated with Cu/SiO₂-TiO₂ nanobiocatalysts. *Mod. Approaches Mater. Sci.* **3**, 374–383 (2020). <https://doi.org/10.32474/MAMS.2020.03.000163>
 - 30 López-Goerne, T., Gracia, A., Padilla-Godínez, F.J., Lottici, P., Silvestre-Albero, A.M.: Characteristic of Ag/TiO₂–SiO₂ bionanocatalysts prepared by sol–gel method as potential antineoplastic compounds. *Bull. Mater. Sci.* **45**(3) (2022). <https://doi.org/10.1007/s12034-021-02570-8> (a)
 - 31 López-Goerne, T., Padilla-Godínez, F.J.: Catalytic Nanomedicine as a Therapeutic Approach to Brain tumors: Main hypotheses for mechanisms of action. *Nanomaterials.* **13**, 1541 (2023). <https://doi.org/10.3390/nano13091541>
 - 32 López-Goerne, T., Ramírez, P., Arévalo, A., Huantes, M., Padilla-Godínez, F.J.: Catalytic Nanomedicine – A new Approach and Solution for Chronic Ulcers: Case Series. *Int J Low Extrem Wounds.* 153473462211190 (b). (2022). <https://doi.org/10.1177/15347346221119006>
 - 33 López-Goerne, T., Rodríguez-Reinoso, F., Padilla-Godínez, F.J., Silvestre-Albero, A.M.: Atomic and electronic composition study of different anticonvulsants stabilized on titania-nanoreservoirs. *Spectrosc. Lett.* **55**, 58–64 (2022). (c) <https://doi.org/10.1080/00387010.2022.2026404>
 - 34 López-Goerne, T.M., Padilla-Godínez, F.J., Álvarez, D., Gómez, E., Ramírez, P., Barragán, E., Chico-Ponce de León, F., González-Carranza, V., García-Beristain, J.C., Dies-Suárez, P., Manrique, J.C.: Titania-Platinum Nanobiocatalyst as Treatment for Central Nervous System tumors: A Case Report on a Pediatric Ependymoma. *J. Neurol. Neurocritical Care.* **3**, 1–8 (2020). <https://doi.org/10.31038/JNNC.2020312>
 - 35 López-Goerne, T.M., Padilla-Godínez, F.J., Castellanos, M., Perez-Davalos, L.A.: Catalytic nanomedicine: a brief review of bionanocatalysts. *Nanomedicine.* **17**, 1131–1156 (d). (2022). <https://doi.org/10.2217/nnm-2022-0027>
 - 36 Maaz, M., Elzein, T., Dragoe, D., Bejjani, A., Jarroux, N., Poulard, C., Aubry-Barroca, N., Nsouli, B., Roger, P.: Poly(4-vinylpyridine)-modified silica for efficient oil/water separation. *J. Mater. Sci.* **54**, 1184–1196 (2019). <https://doi.org/10.1007/s10853-018-2888-x>
 - 37 Meškiniš, Š., Tamulevičius, S., Kopustinskas, V., Andrulevičius, M., Guobienė, A., Gudaitis, R., Liutvinienė, I.: Hydrophobic properties of the ion beam deposited DLC films containing SiO_x. *Thin Solid Films.* **515**, 7615–7618 (2007). <https://doi.org/10.1016/j.tsf.2006.11.089>
 - 38 Meškiniš, Š., Vasiliauskas, A., Andrulevičius, M., Peckus, D., Tamulevičius, S., Viskontas, K.: Diamond like Carbon films Containing Si: Structure and nonlinear Optical properties. *Materials.* **13**, 1003 (2020). <https://doi.org/10.3390/ma13041003>
 - 39 Montemurro, N.: Glioblastoma Multiforme and genetic mutations: The issue is not over yet. An overview of the current literature. *J. Neurol. Surg. Cent. Eur. Neurosurg.* **81**, 064–070 (2020). <https://doi.org/10.1055/s-0039-1688911>
 - 40 Muñoz, E., Boldú, J.L., Andrade, E., Novaro, O., Bokhimi, X., López, T., Gómez, R.: Intrinsically formed trivalent Titanium ions in Sol–Gel Titania. *J. Am. Ceram. Soc.* **84**, 392–398 (2001). <https://doi.org/10.1111/j.1151-2916.2001.tb00667.x>
 - 41 Naeem, M., Hasanain, S.K., Kobayashi, M., Ishida, Y., Fujimori, A., Buzby, S., Shah, S.I.: Effect of reducing atmosphere on the magnetism of zn 1–x Co x O (0 ≤ x ≤ 0.10) nanoparticles. *Nanotechnology.* **17**, 2675–2680 (2006). <https://doi.org/10.1088/0957-4484/17/10/039>
 - 42 Navarrete, J., Lopez, T., Gomez, R., Figueras, F.: Surface acidity of Sulfated TiO₂–SiO₂ Sol-Gels. *Langmuir.* **12**, 4385–4390 (1996). <https://doi.org/10.1021/LA950927Q>
 - 43 Padilla-Godínez, F.J., Ramírez, P., Cruz, R., Sánchez, I., de la Rosa, J.M., López-Goerne, T.: Cytotoxic effect of bionanocatalysts evaluated by diffuse reflectance spectroscopy in an in vivo model of hepatocellular carcinoma. *Results Chem.* **5**, 100894 (2023). <https://doi.org/10.1016/j.rechem.2023.100894>
 - 44 Pan, Y., Monje, M.: Neuron–glial interactions in Health and Brain Cancer. *Adv. Biol.* **6** (2022). <https://doi.org/10.1002/adbi.202200122>
 - 45 Poulston, S., Parlett, P.M., Stone, P., Bowker, M.: Surface oxidation and reduction of CuO and Cu₂O studied using XPS and XAES. *Surf. Interface Anal.* **24**, 811–820 (1996). [https://doi.org/10.1002/\(SICI\)1096-9918\(199611\)24:12%3C811::AID-SIA191%3E3.0.CO;2-Z](https://doi.org/10.1002/(SICI)1096-9918(199611)24:12%3C811::AID-SIA191%3E3.0.CO;2-Z)

- 46 Sadiq, R., Khan, Q.M., Mobeen, A., Shah, A.: Genotoxicity of aluminium oxide, iron oxide, and copper nanoparticles in mouse bone marrow cells. *Archives Industrial Hygiene Toxicol.* **72**, 315–325 (2021). <https://doi.org/10.2478/aiht-2021-72-3578>
- 47 Skoda, F., Astier, M.P., Pajonk, G.M., Primet, M.: Surface characterization of palladium-copper bimetallic catalysts by FTIR spectroscopy and test reactions. *Catal. Lett.* **29**, 159–168 (1994). <https://doi.org/10.1007/BF00814262>
- 48 Slegers, R.J., Blumcke, I.: Low-grade developmental and epilepsy associated brain tumors: A critical update 2020. *Acta Neuropathol. Commun.* **8**, 27 (2020). <https://doi.org/10.1186/s40478-020-00904-x>
- 49 Taylor, O.G., Brzozowski, J.S., Skelding, K.A.: Glioblastoma Multiforme: An overview of emerging therapeutic targets. *Front. Oncol.* **9** (2019). <https://doi.org/10.3389/fonc.2019.00963>
- 50 Walch, H., Dienstmaier, J., Eder, G., Gutzler, R., Schlögl, S., Sirtl, T., Das, K., Schmittl, M., Lackinger, M.: Extended two-Dimensional Metal–Organic frameworks based on thiolate–copper coordination bonds. *J. Am. Chem. Soc.* **133**, 7909–7915 (2011). <https://doi.org/10.1021/ja200661s>
- 51 Wang, C., Youle, R.J.: The role of Mitochondria in apoptosis. *Annu. Rev. Genet.* **43**, 95–118 (2009). <https://doi.org/10.1146/annurev-genet-102108-134850>
- 52 Wang, J.A., Bokhimi, X., Novaro, O., López, T., Tzompantzi, F., Gómez, R., Navarrete, J., Llanos, M.E., López-Salinas, E.: Effects of structural defects and acid–basic properties on the activity and selectivity of isopropanol decomposition on nanocrystallite sol–gel alumina catalyst. *J. Mol. Catal. Chem.* **137**, 239–252 (1999). [https://doi.org/10.1016/S1381-1169\(98\)00077-6](https://doi.org/10.1016/S1381-1169(98)00077-6)
- 53 Wang, J.-C., Zhang, L., Fang, W.-X., Ren, J., Li, Y.-Y., Yao, H.-C., Wang, J.-S., Li, Z.-J.: Enhanced Photoreduction CO₂ activity over Direct Z-Scheme α -Fe₂O₃/Cu₂O Heterostructures under visible light irradiation. *ACS Appl. Mater. Interfaces.* **7**, 8631–8639 (2015). <https://doi.org/10.1021/acsami.5b00822>
- 54 Wang, L., Azad, N., Kongkanermit, L., Chen, F., Lu, Y., Jiang, B.-H., Rojanasakul, Y.: The Fas Death Signaling Pathway connecting reactive Oxygen species Generation and FLICE inhibitory protein down-regulation. *J. Immunol.* **180**, 3072–3080 (2008). <https://doi.org/10.4049/jimmunol.180.5.3072>
- 55 Wang, T.-H., Gole, J.L., White, M.G., Watkins, C., Street, S.C., Fang, Z., Dixon, D.A.: The surprising oxidation state of fumed silica and the nature of water binding to silicon oxides and hydroxides. *Chem. Phys. Lett.* **501**, 159–165 (2011). <https://doi.org/10.1016/j.cplett.2010.11.013>
- 56 Wu, W., Klockow, J.L., Zhang, M., Lafortune, F., Chang, E., Jin, L., Wu, Y., Daldrup-Link, H.E.: Glioblastoma Multiforme (GBM): An overview of current therapies and mechanisms of resistance. *Pharmacol. Res.* **171**, 105780 (2021). <https://doi.org/10.1016/j.phrs.2021.105780>
- 57 Zamora, M., López, T., Asomoza, M., Meléndrez, R., Gómez, R.: Alkaline doped TiO₂ sol–gel catalysts: Effect of sintering on catalyst activity and selectivity for acetone condensation. *Catal. Today.* **116**, 234–238 (2006). <https://doi.org/10.1016/J.CATTOD.2006.02.087>

Publisher's Note Springer Nature remains neutral with regard to jurisdictional claims in published maps and institutional affiliations.